Macromolecules

pubs.acs.org/Macromolecules Article

Excluded Volume of Slide Rings in Single-Chain Polyrotaxane

Jinyuan Mao, Xiang-Meng Jia,* Guojie Zhang, and Jiajia Zhou*

Cite This: *Macromolecules* 2024, 57, 3841−3849 Read Online

ACCESS | Metrics & More | Article Recommendations | Supporting Information

ABSTRACT: We investigate the influence of slide rings on the stretching behavior of a single-chain polyrotaxane anchored by a fix ring. The extension of the force side in our simulations is in line with the previous theoretical framework. However, the end-to-end distance on the free side shows a discrepancy. To address this, we include the excluded-volume effect, successfully aligning with theoretical predictions. We propose a comprehensive model that incorporates excluded-volume effects for rings on both the free side and the force side. The model demonstrates qualitative consistency with simulation data, highlighting the competition among rings from each side. The force-side rings exert a significant influence on the extension of the force side, as derived from the excluded-volume effects. These findings of greater force responsiveness of force-side rings have potential implications for the design of slide-ring gels.

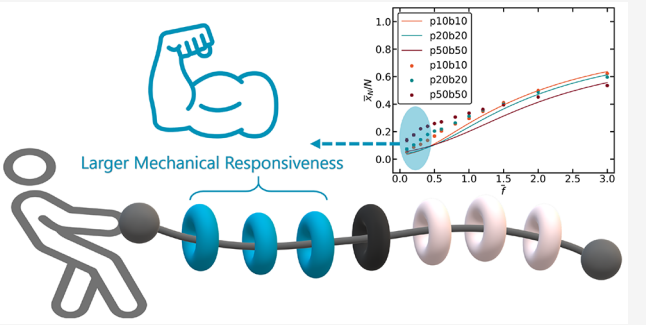

INTRODUCTION

Mechanically interlocked polymers (MIPs) have recently emerged as a novel class of polymer architecture featured with mechanical bonds, which are formed between two or more topological interlocking molecular components without covalent bonds.[1,2] Mechanically interlocked molecules (MIMs) exhibit substantial conformational freedom while preserving a persistent spatial association among their components. MIMs have significantly contributed to the realm of molecular switches and molecular machines, earning recognition through the 2016 Nobel Prize in Chemistry.[3−5] Nevertheless, the impact of MIMs reaches far beyond this domain, with extensive investigations ranging from drug delivery to catalysis.[6−10] The common MIP adopts the rotaxane architecture, consisting of a ring (macrocycle) threaded onto a dumbbell-like component. One well-known example of polymeric analogy to this concept is main-chain polyrotaxane, fabricated by threading cyclic molecules onto linear polymer chains.[11−13] Based on main-chain polyrotaxane, the slide-ring materials (SRMs) can be synthesized through intermolecular cross-linking of the cyclic molecules, which exhibits lower Young's modulus and much greater strain at break.[14−17] These characteristics have opened up exciting avenues for advanced polymer research and applications.[1,18] The concept of SRMs was first introduced by Okumura and Ito.[15,19,20] The term slide-ring gels (SRGs), employed to describe these materials, have also been synthesized from main-chain polyrotaxanes. SRGs consist of three components: linear polymer poly(ethylene glycol)s (PEG), cyclic molecule cyclodextrin (CD), and bulky end molecules adamantine. The most prevalent configurations within these systems feature figure-of-eight cross-links. Consequently, the resulting MIP networks possess mobile junctions capable of sliding unrestricted along the linear polymer backbone.

Over the past two decades, extensive research has been conducted on the relationship between the architecture and structural properties of topological SRGs.[21−24] However, the mechanical properties of SRGs continue to perplex researchers due to the unusually weak dependence of modulus (E) on cross-link density (ν). This dependence seems to follow a scaling law of $E \sim \nu^{0.2}$ or $\nu^{0.5}$, rather than the expected $E \sim \nu^{1}$ seen in traditional fixed-cross-linked networks.[16,21,25,26] Furthermore, this dependence is occasionally nonmonotonic.[21] In 1999, de Gennes proposed a theory suggesting that SRGs should exhibit the same modulus at the swelling equilibrium. At this point, the excess degrees of freedom provided by slide cross-links would contribute to swelling the gel rather than reducing the modulus during deformation.[27] Nevertheless, even in traditional networks with fixed cross-links, comprehending network elasticity remains challenging due to issues like defects such as loops and dangling ends.[28]

Due to the complexity of the slide-ring gels, it might be better to first investigate a single-chain polyrotaxane, with the hope that a better understanding of single-chain behavior would help to clarify the mechanical properties of SRGs. Baulin et al. presented theoretical findings on sliding grafted polymer layers without slide rings,[29] whereas Pinson et al.

Received: December 19, 2023
Revised: March 8, 2024
Accepted: April 5, 2024
Published: April 11, 2024

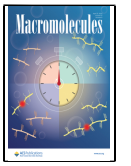

https://doi.org/10.1021/acs.macromol.3c02606
Macromolecules 2024, 57, 3841−3849

introduced slide rings to the single-chain polyrotaxane and observed a remarkable impact on the extension profile of the model.[30] The authors demonstrated that the translational entropy of the slide rings can significantly modify the chain's response to small applied forces. Specifically, if the slide rings are unevenly distributed, the chain can exhibit stiffness at low force levels, and the polyrotaxane chain will stretch beyond a yielding force that scales as $(p/N)^{1/2}$ in a Θ-solvent. Here, p represents the total number of slide rings far from the applied-force terminal, and N is the length of the polyrotaxane chain. Notably, the entropy of the chain becomes the dominant factor, rendering the influence of the slide rings negligible under these large forces.

Tendomers, consisting of pairs of cross-linked rotaxane molecules connected by a slip link, have emerged as a promising system for investigating their mechanical properties. For example, Müller et al. reported the formation of a cluster of tendomers by cross-linking the first slide rings of two rotaxanes between two polymer backbones. To gain insight into the fundamental physics of tendomers, they applied an external force by pulling the two ends of chains adjacent to the slip link. This action compressed the slide rings, impacting the elastic properties of the tendomers. By employing an exact partition function, they modeled the tendomer, accounting for the repulsion between the slide rings and the finite extensibility of the polymer chains. The authors discovered that tendomers exhibit a jump-like mechanical response with a critical pulling force of approximately $(p/N)^{1/2}$ in a symmetric system. Furthermore, these findings can be extended to asymmetric tendomers with varying numbers of slide rings per rotaxane, enabling the design of multistep force−extension profiles with predetermined critical forces.[31−33] However, in a real system, two significant factors, which were either not considered or only partially addressed in previous research, will become crucial. Strain softening, as noted by Pinson et al., becomes most pronounced at higher external applied forces, where the excluded volume between the slide rings becomes relevant.[30] Additionally, the finite extensibility of the polymer chains must also be taken into account.

In this study, we begin by presenting an overview of the current understanding of single-chain polyrotaxane. Subsequently, we conduct a comprehensive investigation into the influence of finite extensibility and excluded volume within a single-chain polyrotaxane model, primarily focusing on the distribution of slide rings. To achieve this, we employed coarse-grained molecular dynamics simulations. Our findings demonstrate strong alignment with theoretical predictions, even when considering finite extensibility under highly external applied forces via the incorporation of Langevin function corrections. Furthermore, we delve into the excluded-volume effects between inter-rings, which have a notable impact on the yielding force. Additionally, we identify a competition of rings from both sides within this single-chain polyrotaxane model.

SIMULATION MODEL

In this study, we employed coarse-grained (CG) molecular dynamics simulations of the Kremer−Grest model[34] to elucidate the mechanical response within a main-chain polyrotaxane. Figure 1 illustrates the schematic representation of the CG model for the single-chain polyrotaxane, which consists of distinct components, namely, the free end, polymer backbone, slide ring, fix ring, and force end. The polymer backbone of the polyrotaxane chain was coarse-grained as a

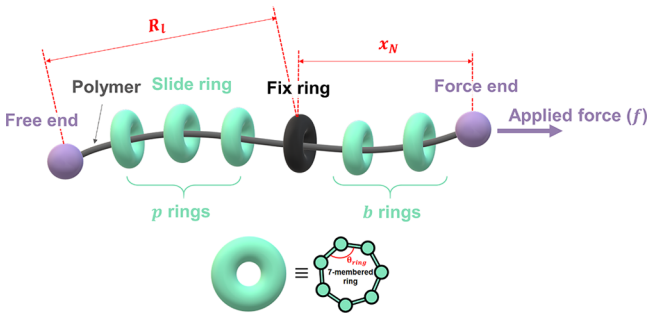

Figure 1. Schematic illustration of a single-chain polyrotaxane model.

linear bead−spring polymer chain with a chain length of N = 400. The slide ring was represented as a relatively rigid ring composed of seven beads. The fix ring remained stationary and functioned to separate the slide-ring components distributed in space. The free end and force end were positioned at the two termini of the linear polymer backbone to prevent the rings from slipping out. External forces were exclusively applied to the force end. The numbers of the free slide rings on the free side and the force side are denoted by p and b, respectively.

We conducted CG molecular dynamics simulations employing an implicit solvent model within a NVT ensemble, utilizing the GALAMOST package.[35] The total potential energy of our model encompasses both covalent and noncovalent interactions, as well as a bending potential component, and can be defined as follows:

$$E_{\text{total}} = E_{\text{b}} + E_{\text{nb}} + E_{\text{bend}} \tag{1}$$

The covalent bond is described by the finitely extensible nonlinear elastic (FENE) spring potential

$$E_{\text{b}}(r) = -\frac{1}{2}k_{\text{b}}{r_{\text{max}}}^2 \ln\left(1 - \frac{r^2}{{r_{\text{max}}}^2}\right) \tag{2}$$

where the spring constant k_{b} is set to 30.0 ε/σ^2 and r is the instantaneous bond length with its maximum bond extension r_{max} = 1.5 σ.

The nonbonded interactions E_{nb} are described by Weeks−Chandler−Andersen (WCA) potential[36]

$$E_{\text{nb}}(r_{ij}) = \begin{cases} 4\varepsilon\left[\left(\frac{\sigma}{r_{ij}}\right)^{12} - \left(\frac{\sigma}{r_{ij}}\right)^{6}\right] + \varepsilon & , r_{ij} \le \sqrt[6]{2}\sigma \\ 0 & , r_{ij} > \sqrt[6]{2}\sigma \end{cases} \tag{3}$$

where r_{ij} is the distance between one pair of monomers. The ε and σ are energy and length scales, which are set to unity for convenience. Specifically, by turning off the nonbonded interactions among non-neighboring polymer backbone beads, the simulated system is in a Θ-solvent condition (Figure S1 in the Supporting Information). The free end and force end are represented by a single bead of a larger radius. The interaction between the end beads and the ring beads is given by

https://doi.org/10.1021/acs.macromol.3c02606
Macromolecules 2024, 57, 3841−3849

$$E_{nb}(r_{ij}) = \begin{cases} 4\varepsilon\left[\left(\frac{\sigma}{r_{ij}-\Delta}\right)^{12} - \left(\frac{\sigma}{r_{ij}-\Delta}\right)^{6}\right] + \varepsilon & , r_{ij} \le \sqrt[6]{2}\sigma + \Delta \\ 0 & , r_{ij} > \sqrt[6]{2}\sigma + \Delta \end{cases} \quad (4)$$

where $\Delta = R_i + R_j - \sigma$. Specifically, the radius of the end bead is set as $R = 1.5\ \sigma$ and the radius of the ring bead is $R = 0.5\ \sigma$. In our simulations, the mass of one CG bead is denoted as m, and we used standard reduced units with $\sigma = \varepsilon = m = 1.0$ and time scale $\tau = (m\sigma^2/\varepsilon)^{1/2}$.

E_{bend} is solely employed for ring beads to preserve the shape of the rings and is described as follows:

$$E_{bend} = \frac{1}{2}k_{ring}(\theta - \theta_{ring})^2 \quad (5)$$

where $k_{ring} = 1000.0\ \varepsilon/rad^2$ is the angle strength and $\theta_{ring} = 5\pi/7$ is the equilibrium angle for three consecutive beads in one ring. The choice of parameters ensures that the diameter of the ring is large enough to enable unimpeded sliding along the polymer backbone.[37,38]

The CG molecular dynamics simulations were conducted by solving the Langevin equation:

$$m\ddot{\mathbf{r}}_i = -\nabla_i E_{total} - \gamma\dot{\mathbf{r}}_i + \boldsymbol{\xi}_i \quad (6)$$

This equation describes the motion of a particle with a mass m in a system. It includes the following terms: $\ddot{\mathbf{r}}_i$ represents the second derivative of the position vector $\mathbf{r}_i$ with respect to time, which is the particle's acceleration; $-\nabla_i E_{total}$ is the force acting on the particle due to the gradient of the total energy E_{total}; $-\gamma\dot{\mathbf{r}}_i$ represents the damping term, where γ is the friction coefficient and $\dot{\mathbf{r}}_i$ is the velocity of the particle; $\boldsymbol{\xi}_i$ is the stochastic force term, which is related to the friction coefficient γ by the fluctuation−dissipation theorem $\langle\boldsymbol{\xi}_i(t)\boldsymbol{\xi}_j(t')\rangle = 2k_BT\gamma\delta_{ij}\delta(t-t')$, where k_B and T are the Boltzmann constant and temperature of the system, respectively. In this study, we set $k_BT = 1.0\ \varepsilon$. The friction coefficient used in this study was $\gamma = 0.5\ m/\tau$. We conducted a prerelaxation process lasting for $10^4\ \tau$, employing an integration time step of $0.005\ \tau$. Following this, a constant force was applied to the force terminal for a duration of $5 \times 10^5\ \tau$, and measurements were performed. (The time series of measured quantities can be found in Figure S2.) We repeated this process to generate the extension−force profiles. For each data point, three independent runs were performed to obtain error bars.

THEORETICAL MODELS AND SIMULATION RESULTS

In this section, we commence our exploration by examining a simple model from Pinson et al. where $p \neq 0$, $b = 0$.[30] To discern the disparities with simulation results of the end-to-end distance on the free side ($\overline{R}_l$), we introduce the scenario of $p \neq 0$, $b = 0$ with the excluded-volume effect of p rings. Subsequently, we delve into the examination of the case where $p \neq 0$, $b \neq 0$. This scenario yields an anomalous phenomenon in the extension of $\overline{x}_N$ under the limit of small applied force. Finally, we propose a comprehensive model of $p \neq 0$, $b \neq 0$ that incorporates excluded-volume effects for both p and b rings.

$p \neq 0$, $b = 0$ without Excluded Volume of Slide Rings. *Pinson's Free Energy Model.* We begin by considering the simplified case where rings are exclusively present on the free side ($p \neq 0$, $b = 0$). Pinson et al. employed a physically simple model[30] to elucidate the required yielding force for stretching a polyrotaxane chain from the force side. In this context, we reproduce their derivation for completeness by using our notation. Ignoring fluctuations, the free energy of a stretched polyrotaxane chain can be expressed as

$$\mathcal{F} = -fx_N + \frac{3k_BT}{2}\frac{x_N^2}{na^2} - k_BTp\ln(N-n) \quad (7)$$

The free energy comprises three components: The first term represents the potential energy resulting from the applied force, fx_N. The second term corresponds to the entropic stretching energy of the force side of the polyrotaxane chain with rings (the subchain is assumed to be Gaussian and is composed of n monomers, each with a size of a). The last term arises from the entropy of the slide rings, which can be expressed as $k_BTp\ln[p/(N-n)] = k_BTp\ln p - k_BTp\ln(N-n)$, with the constant term $p\ln p$ neglected.

The free energy depends on two variables: x_N and n. We first minimize the free energy with respect to x_N

$$\frac{\partial\mathcal{F}}{\partial x_N} = 0 \Rightarrow \frac{x_N}{a} = \frac{n}{3}\left(\frac{fa}{k_BT}\right), \quad \overline{x}_N = \frac{n}{3}\overline{f} \quad (8)$$

We use the dimensionless variables with overbars:

$$\overline{x}_N = \frac{x_N}{a} \quad (9)$$

$$\overline{f} = \frac{fa}{k_BT} \quad (10)$$

The free energy becomes

$$\mathcal{F} = -\frac{na^2f^2}{6k_BT} - k_BTp\ln(N-n) \quad (11)$$

We then minimize eq 11 with respect to n

$$\frac{\partial\mathcal{F}}{\partial n} = -\frac{a^2f^2}{6k_BT} + k_BT\frac{p}{N-n} \quad (12)$$

The preceding equation cannot be equal to zero if $f < f^*$.

$$f^* = \frac{k_BT}{a}\sqrt{\frac{6p}{N}}, \quad \overline{f}^* = \sqrt{\frac{6p}{N}} \quad (13)$$

The equilibrium values of n and x_N are

$$\frac{n}{N} = \begin{cases} 0 & \text{if}\ \overline{f} < \overline{f}^* \\ 1 - \frac{6p}{N}\frac{1}{\overline{f}^2} & \text{if}\ \overline{f} > \overline{f}^* \end{cases} \quad (14)$$

$$\overline{x}_N = \begin{cases} 0 & \text{if}\ \overline{f} < \overline{f}^* \\ \frac{N}{3}\overline{f}\left[1 - \left(\frac{\overline{f}^*}{\overline{f}}\right)^2\right] & \text{if}\ \overline{f} > \overline{f}^* \end{cases} \quad (15)$$

https://doi.org/10.1021/acs.macromol.3c02606
Macromolecules 2024, 57, 3841−3849

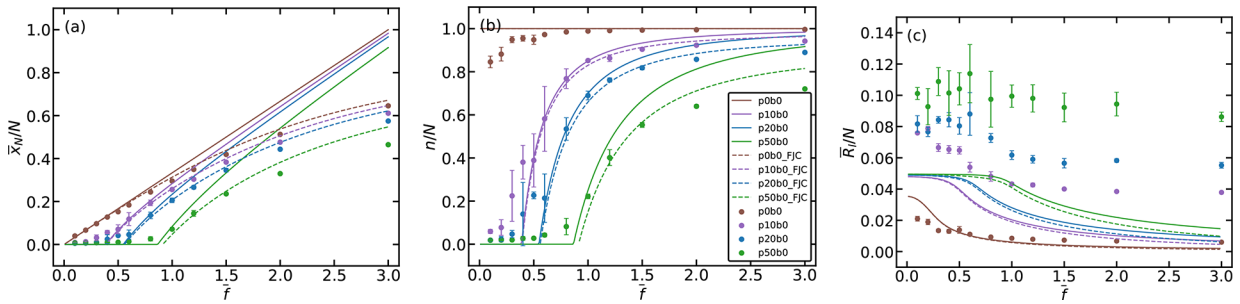

Figure 2. Theoretical predictions (solid line), FJC correction results (dashed line), and simulation results (dots) for a single-chain polyrotaxane model in a Θ-solvent across various scenarios: ($p0$, $p10$, $p20$, $p50$)$b0$. (a) Dimensionless projection of the end-to-end distance in the direction of the applied force ($\overline{x}_N$) as a function of the dimensionless applied force ($\overline{f}$). (b) Number of monomers (n) on the force side as a function of $\overline{f}$. (c) Dimensionless end-to-end distance ($\overline{R}_l$) on the free side as a function of $\overline{f}$. The solid line in (c) represents the expected behavior of the Gaussian chain, specifically $\langle \overline{R}_l^2 \rangle^{1/2} \sim (N-n)^{1/2} a$.

The most important conclusion from this simple model is the existence of a yielding force $\overline{f}^*$. Only when the applied force is greater than $\overline{f}^*$, the polyrotaxane chain started to be stretched.

Correction of average chain elongation by the Langevin function. For small relative elongations, the relationship between average extension and applied force follows Hooke's law ($\overline{x}_N = \overline{f}/3$). However, in the limit of large $\overline{f}$, the Gaussian chain has to be replaced by the freely jointed chain (FJC) for the finite extensibility of polymers by the Langevin function $\mathcal{L}(\overline{f}) = \coth(\overline{f}) - 1/\overline{f}$,[39] that is, $\overline{f} = 3\mathcal{L}(\overline{f})$ should be substituted in eqs 14 and 15 and thus obtaining the FJC-correction data (eqs 16 and 17) in the limit of large force.

$$\frac{n}{N} = \begin{cases} 0 & \text{if } \overline{f} < \overline{f}^* \\ 1 - \dfrac{2p}{3N} \dfrac{1}{[\coth(\overline{f}) - 1/\overline{f}]^2} & \text{if } \overline{f} > \overline{f}^* \end{cases} \tag{16}$$

$$\overline{x}_N = \begin{cases} 0 & \text{if } \overline{f} < \overline{f}^* \\ N[\coth(\overline{f}) - 1/\overline{f}]\left[1 - \dfrac{1}{9}\left[\dfrac{\overline{f}^*}{\coth(\overline{f}) - 1/\overline{f}}\right]^2\right] & \text{if } \overline{f} > \overline{f}^* \end{cases} \tag{17}$$

Simulation Results. We now compare the simulation results to the theoretical predictions. For clarify, we establish the naming convention such as "$p20b0$", indicating the case that the free side has 20 slide rings and the force side has 0 slide rings. First, Figure 2a illustrates the dimensionless extension ($\overline{x}_N = x_N/a$) of the force side as a function of the dimensionless applied force ($\overline{f} = fa/k_BT$) for various values of p (0, 10, 20, and 50), while keeping the number of rings b = 0 (depicted as dots). For the case of p = 0, the behavior closely resembles that of an ideal chain, displaying entropic elasticity and adhering to Hooke's law at low applied forces. However, as the number of slide rings increases (e.g., p = 10, 20, and 50), a yielding force ($\overline{f}^*$) emerges. In a fashion analogous to osmotic pressure, the monomers in this scenario play the role of a solvent, while the p slide rings represent a region of higher solute concentration. This configuration effectively hinders the passage of monomers across the fix ring, maintaining an osmotic balance until the externally applied force exceeds the yielding force ($\overline{f} > \overline{f}^*$). These observations align with the theoretical perspectives put forth by Pinson et al.,[30] especially in the regime of low applied forces (solid line in Figure 2a). However, it is important to note that the Gaussian approximation becomes less applicable at higher forces. In such cases, the FJC model must be employed.[31] To address this, we adjusted the curves using the Langevin function (dashed line in Figure 2a). In summary, our simulation results for the dimensionless extension ($\overline{x}_N$) as a function of the dimensionless applied force ($\overline{f}$) are in excellent agreement with the theoretical predictions, both in the low-force regime and even in the high-force limit when considering the finite extensibility of the polymer chain.

We can further explore the mean response of the polyrotaxane chain to the applied force ($\overline{f}$). When subjected to an applied force, the mean number of monomers (n) on the force side may deviate from the expression given in eq 14. In this context, we present the plot of n as a function of $\overline{f}$ for scenarios with different values of p (0, 10, 20, and 50) but no slide rings (b = 0) in the force side, as shown in Figure 2b. It is worth noting that the theoretical results have previously been studied by Pinson et al.[30] in their investigation of the equilibrium properties of a single polyrotaxane with a series of rings. Specifically, we employ the Langevin function to account for the correction in the number of rings n. The simulation results presented in Figure 2b (depicted as dots) for these scenarios are consistent with their findings. The plot in Figure 2b reveals that as $\overline{f}$ increases, the value of n also increases for all scenarios. This behavior can be attributed to the fact that the polyrotaxane becomes more extended under higher applied forces. As expected, the values of n decrease with an increasing number of p rings. This reduction is due to the presence of p rings, leading to steric hindrance and a reduction in the available space for the sliding motion of the rings.

However, upon observing the end-to-end distance on the free side ($\overline{R}_l$ in Figure 1) as a function of $\overline{f}$, we observe a substantial inconsistency: the simulation results significantly surpass the theoretical values when taking into consideration that the chain on the free side is also modeled as a Gaussian chain (solid line in Figure 2c) and corrected by the Langevin function (dashed line in Figure 2c). In light of this, we contemplate that the influence of excluded-volume effects of the slide rings has a significant impact on $\overline{R}_l$.

https://doi.org/10.1021/acs.macromol.3c02606
Macromolecules 2024, 57, 3841−3849

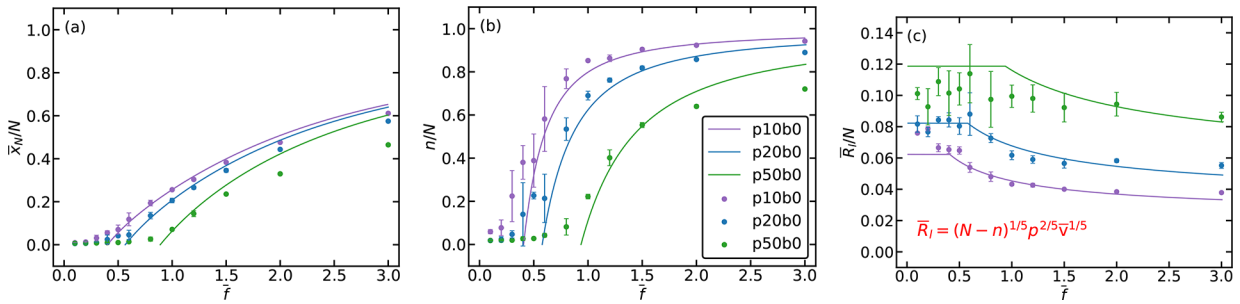

Figure 3. Excluded-volume version of theoretical predictions (solid line) and simulation results (dots) for a single-chain polyrotaxane model in a Θ-solvent across various scenarios: (p10, p20, and p50)b0. (a) Dimensionless projection of the end-to-end distance in the direction of the applied force ($\bar{x}_N$) as a function of the dimensionless applied force ($\bar{f}$). (b) Number of monomers (n) on the force side as a function of $\bar{f}$. (c) Dimensionless end-to-end distance ($\bar{R}_l$) on the free side as a function of $\bar{f}$. The solid line in (c) represents values derived from the equation $\bar{R}_l = (N-n)^{1/5} p^{2/5} \bar{v}^{1/5}$ as given in eq 20, with $\bar{v} \approx 17.7$.

$p \neq 0$, $b = 0$ with Excluded Volume of Slide Rings. *Including Excluded Volume of p Rings.* The standard theory of excluded volume was introduced by Flory. In Flory theory, N monomers of a polymer chain in a good solvent are assumed to be uniformly distributed within a volume of R^3 without mutual correlations. The enthalpic contribution to the free energy is given by $F_{\text{int}} \approx k_B T v N^2/R^3$, where v is the excluded volume.[39] The entropic contribution to the free energy is estimated as the energy required to stretch an ideal chain to an end-to-end distance of R, which is given by $F_{\text{ent}} \approx k_B T R^2/Nb^2$.[39]

Here we introduce the excluded-volume interaction among rings but assume the backbone chain remains Gaussian. This is done by adding two more terms to the free energy (eq 7).

$$\mathcal{F} = -fx_N + \frac{3k_BT}{2}\frac{{x_N}^2}{na^2} - k_BTp\ln(N-n) + \frac{3k_BT}{2}\frac{{R_l}^2}{(N-n)a^2} + k_BT\bar{v}a^3\frac{p^2}{{R_l}^3} \tag{18}$$

The second last term is the entropic free energy of the chain on the free side: The end-to-end distance between the free end and the fix ring is R_l, and there are $N-n$ monomers. The last term is the excluded-volume interaction of p rings, assuming the excluded volume of one ring is $\bar{v}a^3$.

The free energy now depends on three variables: x_N, n, and R_l. Minimizing the free energy (18) with respect to x_N leads to the same equation as before.

$$\frac{\partial \mathcal{F}}{\partial x_N} = 0 \Rightarrow \frac{x_N}{a} = \frac{n}{3}\left(\frac{fa}{k_BT}\right), \quad \bar{x}_N = \frac{n}{3}\bar{f} \tag{19}$$

Minimizing the free energy (18) with respect to R_l gives

$$\frac{\partial \mathcal{F}}{\partial R_l} = 0 \Rightarrow \frac{R_l}{a} = (N-n)^{1/5}p^{2/5}\bar{v}^{1/5}, \quad \bar{R}_l = (N-n)^{1/5}p^{2/5}\bar{v}^{1/5} \tag{20}$$

The free energy becomes

$$\mathcal{F} = -\frac{na^2f^2}{6k_BT} - k_BTp\ln(N-n) + \frac{5}{2}k_BT(N-n)^{-3/5}p^{4/5}\bar{v}^{2/5} \tag{21}$$

We then minimize the above free energy with respect to n

$$\frac{\partial \mathcal{F}}{\partial n} = -\frac{a^2f^2}{6k_BT} + k_BT\frac{p}{N-n} + \frac{3}{2}k_BT(N-n)^{-8/5}p^{4/5}\bar{v}^{2/5} \tag{22}$$

The preceding equation cannot be equal to zero if $f < f^*$

$$f^* = \frac{k_BT}{a}\sqrt{\frac{6p}{N} + \frac{9p^{4/5}}{N^{8/5}}\bar{v}^{2/5}}, \quad \bar{f}^* = \sqrt{\frac{6p}{N} + \frac{9p^{4/5}}{N^{8/5}}\bar{v}^{2/5}} \tag{23}$$

From eq 23, we can infer that the yielding force of $\bar{f}^*$ incorporates the term of excluded volume, given by $9p^{4/5}\bar{v}^{2/5}/N^{8/5}$, when compared to eq 13 of Pinson et al.'s results.

The chain will take the following state:

$$n = 0, \quad x_N = 0, \quad \bar{R}_l = N^{1/5}p^{4/5}\bar{v}^{2/5} \tag{24}$$

If the external force is large, $\bar{f} > \bar{f}^*$, we need to solve the equation for n by the numerical method

$$-\frac{\bar{f}^2}{6} + \frac{p}{N-n} + \frac{3}{2}\frac{p^{4/5}}{(N-n)^{8/5}}\bar{v}^{2/5} = 0 \tag{25}$$

Notably, eq 25 can be regarded as $\bar{f}$ as a function of n, where the monomer n is specified as 0 to $N = 400$, and the solution for $\bar{f}$ can be obtained. Subsequently, $\bar{x}_N$ and $\bar{R}_l$, as defined by eqs 19 and 20, can be sequentially solved.

Simulation Results. Figure 3a illustrates the excluded-volume versions of theoretical predictions (solid line) and simulation results (dots) for a single-chain polyrotaxane model in a Θ-solvent under various scenarios: (p10, p20, and p50)b0. It is evident from Figure 3a and Figure 3b that the extension ($\bar{x}_N$) and the average number of monomers (n) on the free side closely align with the theoretical results.

Notably, Figure 3c showcases a remarkable concurrence of $\bar{R}_l$ versus $\bar{f}$ when we account for the excluded volume of p rings. Specifically, we consider an excluded volume of approximately $\bar{v} \approx 17.7$, which corresponds to seven-membered rings as depicted in Figure 1. In this context, the 7-membered rings are treated as a collective unit, and their excluded volume is computed based on the assumption that the space they occupy closely resembles a sphere with a radius of approximately 1.62 σ in our simulation model. The estimated excluded volume for this unit is approximately

https://doi.org/10.1021/acs.macromol.3c02606
Macromolecules 2024, 57, 3841−3849

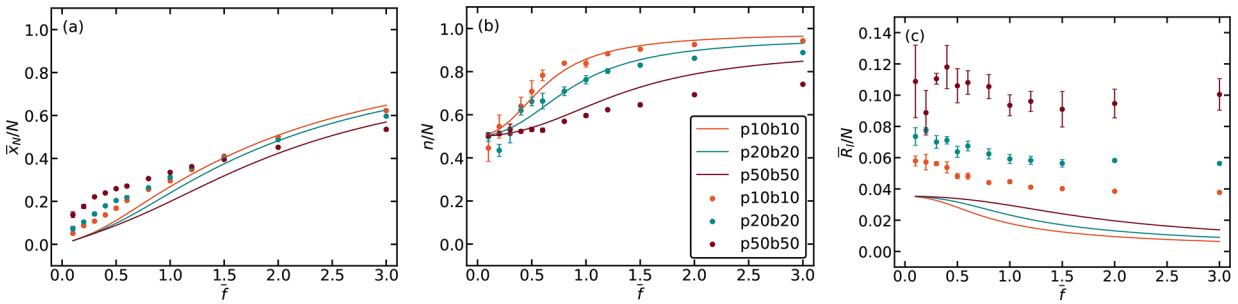

Figure 4. Theoretical predictions (solid line) and simulation results (dots) for a single-chain polyrotaxane model in a Θ-solvent when $p = b$ for 10, 20, and 50. (a) Dimensionless projection of the end-to-end distance in the direction of the applied force ($\bar{x}_N$) as a function of the dimensionless applied force ($\bar{f}$). (b) Number of monomers (n) on the force side as a function of $\bar{f}$. (c) Dimensionless end-to-end distance ($\bar{R}_l$) on the free side as a function of $\bar{f}$. The solid line in (c) represents the expected behavior of the Gaussian chain, specifically $\langle \bar{R}_l^{\,2} \rangle^{1/2} \sim (N-n)^{1/2} a$.

$\bar{v}a^3 = 4/3\pi R^3 \approx 17.7\,\sigma^3$. (The detailed calculation can be found in Figure S3.)

***p* ≠ 0, *b* ≠ 0 without Excluded Volume of Slide Rings.** *b Rings in Simple Model.* In this subsection, we aim to introduce b rings, which are interlocked between the fix ring and the force end (Figure 1). Moreover, we consider the entropic stretching energy of the subchain containing b rings as a Gaussian subchain within this simplified model. As a consequence, eq 7 of ideal free energy should be rewritten as

$$\mathcal{F} = -fx_N + \frac{3k_BT}{2}\frac{x_N^{\,2}}{na^2} - k_BT[p\ln(N-n) + b\ln n] \tag{26}$$

The minimization of x_N, the extension of the force side subchain, or $\partial\mathcal{F}/\partial x_N = 0$, yields an equilibrium extension

$$\frac{\partial \mathcal{F}}{\partial x_N} = 0 \Rightarrow \frac{x_N}{a} = \frac{n}{3}\left(\frac{fa}{k_BT}\right), \quad \bar{x}_N = \frac{n}{3}\bar{f} \tag{27}$$

and a free energy of

$$\mathcal{F} = -\frac{na^2f^2}{6k_BT} - k_BT[p\ln(N-n) + b\ln n] \tag{28}$$

We now minimize this over the number of monomers (n) in the stretched ringless subchain of the force side. It diverges when $n \to 0$, and the applied force can be obtained:

$$f = \frac{k_BT}{a}\sqrt{6\left(\frac{p}{N-n} - \frac{b}{n}\right)}, \quad \bar{f} = \sqrt{6\left(\frac{p}{N-n} - \frac{b}{n}\right)} \tag{29}$$

Equation 29 indicates that the applied force is influenced by the presence of p and b rings, with p rings enhancing the force and b rings suppressing it. When $p/(N-n) = b/n$, the applied force ($\bar{f}$) is zero, which means that the subchain of force side can be effectively stretched by an arbitrary applied force.

Simulation Results. As depicted in Figure 4a, we present a comparative analysis of theoretical predictions (solid line) and simulation results (dots) for a single-chain polyrotaxane model in a Θ-solvent with varying $p = b$ values, specifically 10, 20, and 50. The simulation results reveal outcomes that contradict the theoretical predictions. At low force limits, as the value of $p = b$ increases, the extension $\bar{x}_N$ in the simulation results remains significantly higher, in stark contrast to the lower values suggested by theoretical predictions. Nevertheless, this observation does not find support in the results presented in Figure 4b, where it becomes evident that the slide rings consistently exhibit lower values of n as the parameter $p = b$ increases. Upon examining the end-to-end distance on the free side ($\bar{R}_l$ in Figure 4c) as a function of $\bar{f}$, we also note the same inconsistencies as observed in Figure 2c, where the prediction from the Gaussian chain underestimated $\bar{R}_l$. This discrepancy is likely attributed to the excluded-volume effects of the slide rings. Here we presented results for symmetric distribution of rings ($p = b$). For the case of asymmetric distribution ($p \neq b$), a similar conclusion can be made (Figures S4 and S5).

***p* ≠ 0, *b* ≠ 0 with Excluded Volume of Slide Rings.** *Including Excluded Volume of Both p and b Rings.* Now, we consider introducing the excluded-volume effects of the p and b slide rings. The state of the polyrotaxane chain is characterized by four variables: n, which represents the number of monomers on the force side; x_N, which signifies the x-axis distance from the force end to the fix ring; y_N, representing the distance perpendicular to the x-axis; and R_l, denoting the distance from the free end to the fix ring. The subchain on the force side resembles a prolate spheroid with its long axis on the x-direction.

The free energy of the system is expressed as follows:

$$\mathcal{F} = -fx_N + \frac{3k_BT}{2}\frac{x_N^{\,2}}{na^2} + \frac{3k_BT}{2}\frac{2y_N^{\,2}}{na^2} + k_BT\bar{v}a^3\frac{b^2}{x_N y_N^{\,2}} - k_BTb \ln n + \frac{3k_BT}{2}\frac{R_l^{\,2}}{(N-n)a^2} + k_BT\bar{v}a^3\frac{p^2}{R_l^{\,3}} - k_BTp\ln(N-n) \tag{30}$$

Minimizing this free energy with respect to R_l

$$\frac{\partial \mathcal{F}}{\partial R_l} = 0 \Rightarrow \frac{R_l}{a} = (N-n)^{1/5}p^{2/5}\bar{v}^{1/5}, \quad \bar{R}_l = (N-n)^{1/5}p^{2/5}\bar{v}^{1/5} \tag{31}$$

The first two terms in the second line of free energy (30) becomes

$$\frac{5}{2}k_BT(N-n)^{-3/5}p^{4/5}\bar{v}^{2/5} \tag{32}$$

Minimizing this free energy with respect to y_N and x_N

https://doi.org/10.1021/acs.macromol.3c02606
Macromolecules 2024, 57, 3841−3849

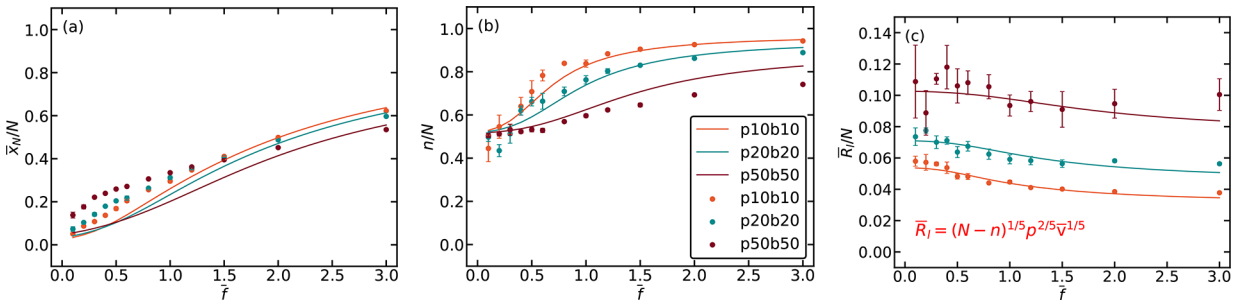

Figure 5. Theoretical predictions (solid line) with the excluded-volume effects of both p and b rings, and simulation results (dots) are presented for a single-chain polyrotaxane model in a Θ-solvent with $p = b$ values of 10, 20, and 50. (a) Dimensionless projection of the end-to-end distance in the direction of the applied force ($\bar{x}_N$) as a function of the dimensionless applied force ($\bar{f}$). (b) Number of monomers (n) on the force side as a function of $\bar{f}$. (c) Dimensionless end-to-end distance ($\bar{R}_l$) on the free side as a function of $\bar{f}$. The solid line in (c) represents values derived from the equation $\bar{R}_l = (N-n)^{1/5}p^{2/5}\bar{v}^{1/5}$ as given in eq 31, with $\bar{v} \approx 17.7$.

$$\frac{\partial \mathcal{F}}{\partial y_N} = 0 \Rightarrow 6k_BT\frac{y_N}{na^2} - 2k_BT\bar{v}a^3\frac{b^2}{x_N {y_N}^3} = 0$$

$$\Rightarrow {\bar{y}_N}^2 = \frac{1}{\sqrt{3}}n^{1/2}\bar{v}^{1/2}{\bar{x}_N}^{-1/2}b,\ \bar{y}_N = \frac{y_N}{a} \tag{33}$$

$$\frac{\partial \mathcal{F}}{\partial x_N} = 0 \Rightarrow -f + 3k_BT\frac{x_N}{na^2} - k_BT\bar{v}a^3\frac{b^2}{{x_N}^2{y_N}^2} = 0$$

$$\Rightarrow {\bar{x}_N}^{5/2} - \frac{n\bar{f}}{3}{\bar{x}_N}^{3/2} - \frac{1}{\sqrt{3}}n^{1/2}\bar{v}^{1/2}b = 0,\ = \frac{x_N}{a} \tag{34}$$

Substituting eq 33 into the free energy (eq 30), the third and fourth terms in the first line of the free energy (eq 30) become

$$2\sqrt{3}\,k_BT[\bar{v}/(\bar{x}_N n)]^{1/2}b \tag{35}$$

Finally, the free energy (eq 30) can be rewritten as

$$\mathcal{F} = -fx_N + \frac{3k_BT}{2}\frac{{x_N}^2}{na^2} + 2\sqrt{3}\,k_BT[\bar{v}/(\bar{x}_N n)]^{1/2}b - k_BTb\ln n + \frac{5}{2}k_BT(N-n)^{-3/5}p^{4/5}\bar{v}^{2/5} - k_BTp\,\ln(N-n) \tag{36}$$

Equation 36 represents the free energy $\mathcal{F}$ as a function of $\bar{x}_N$ and n. By substituting eq 34 into eq 36, one can derive $\mathcal{F}$ as a function of n alone for a specific value of f, p, and b. Here, we employ the numerical method of Sequential Least Squares Programming (SLSQP) from the SciPy package to minimize the free energy of eq 36. The value of n is a constraint between 0 and $N = 400$. The initial values of x_N and n were set to 100 and 350.

Simulation Results. Similarly, we present curves representing the dependencies of $\bar{x}_N$, n, and $\bar{R}_l$ on $\bar{f}$. From Figure 5a, it is evident that we qualitatively capture the relationship between $\bar{x}_N$ and $\bar{f}$ when considering the excluded-volume effects of the p and b slide rings, as compared to Figure 4a where the excluded volume of the p and b slide rings was neglected. The excluded-volume version of this model exhibits trends consistent with the simulation data. Despite some discrepancies in numerical values, this could be attributed to our representation of the excluded volume for all rings as a unified expression ($k_BT\bar{v}a^3\text{rings}^2/R^3$, where rings represents the total number of rings in the polyrotaxane), while neglecting the repulsive interactions between the rings and the chain. Furthermore, as observed in Figure 5c, the simulation results for $\bar{R}_l$ are in close agreement with the theoretical predictions. This indicates a certain degree of accuracy in the excluded-volume model. Furthermore, good agreement between the simulation and theory is also found for asymmetric distribution of rings (Figures S6 and S7). We also studied slide rings of different radius, and the results can also be found in Figure S8.

In more detail, we plot the $\bar{x}_N$ vs $\bar{f}$ when $p = 0$ but $b \neq 0$ (Figure 6). Under low applied forces, the extension ($\bar{x}_N$) increases with the growing value of b rings. While as previously discussed (eq 23), when $p \neq 0$ but $b = 0$, a yielding force is obtained. In the limit of small applied force, specifically below the yielding force, the p rings prevent the monomers on the free side from moving to the force side. In contrast, the b rings enhance the mobility of monomers from the free side to the force side, and in this competition, the b rings have a slight advantage. This competition between the b rings and p rings is the underlying reason for the higher simulation values of $\bar{x}_N$ observed in Figure 5a compared to the theoretical predictions.

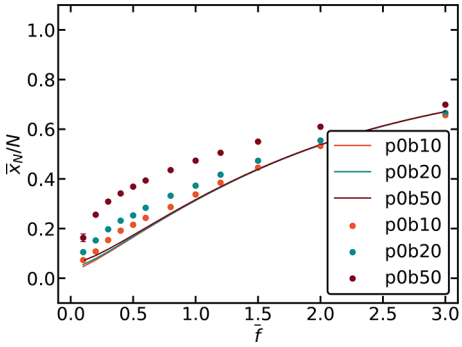

Figure 6. Dimensionless projection of the end-to-end distance in the direction of the applied force ($\bar{x}_N$) as a function of the dimensionless applied force ($\bar{f}$). Theoretical predictions (solid line) take into account the excluded-volume effects of both p and b rings, and simulation results (dots) are presented for a single-chain polyrotaxane model in a Θ-solvent with $p = 0$ but b values of 10, 20, and 50.

CONCLUSIONS

In this paper, we examined the stretching behavior of a single-chain polyrotaxane, comprising slide rings and a single fix ring. The slide rings exhibit significant translational entropy, confined along one dimension of the polymer chain, with

https://doi.org/10.1021/acs.macromol.3c02606
Macromolecules 2024, 57, 3841−3849

their entropy being influenced by the presence of the fix ring. We begin by providing a review of prior research and subsequently introduce the impact of the excluded-volume effects of rings within the single-chain polyrotaxane model. Concurrently, we utilized coarse-grained (CG) molecular dynamics simulations to elucidate the mechanical response within the single-chain polyrotaxane.

Our simulation results consistently align with the theoretical predictions of previous research, even when accounting for finite extensibility under high applied forces ($\overline{f}$) by integrating Langevin function corrections. However, the end-to-end distance of the free side ($\overline{R}_l$) could not be determined within the framework of this simplified single-chain polyrotaxane model. To address this limitation, we introduced the excluded-volume term of p inter-rings in the scenario where $p \neq 0$ but $b = 0$, enabling us to accurately establish the relationship between $\overline{R}_l$ and $\overline{f}$.

Furthermore, when considering the introduction of b rings on the force side, without accounting for the excluded-volume effects of the rings, we could not establish the correct relationship between the extension ($\overline{x}_N$) on the force side and the applied force ($\overline{f}$). Finally, we extended our exploration to a comprehensive version of the single-chain polyrotaxane model, which included the excluded-volume effects of both p and b rings on the free side and force side, respectively. The excluded-volume version of this single-chain polyrotaxane model exhibits trends that are qualitatively consistent with the simulation data, revealing a competition among rings on two sides of the polyrotaxane model. In conclusion, our findings suggest that the rings on the force side have a more significant impact on $\overline{x}_N$ than the rings on the free side due to the influence of the excluded-volume effects. This implies that the responsiveness of the b rings on the force side is greater than that of the p rings on the free side under low applied forces. These findings could contribute to an enhanced understanding of the mechanical properties when designing slide-ring gels. For instance, in the case of incompletely cross-linked slide-ring gels, it is anticipated that the extension of $\overline{x}_N$ will increase with an increase in the number of p and b rings under small applied force. In detail, one can derive the end-to-end distance of free side $\overline{R}_l$ if the subchain of the gel is regarded as a single-chain polyrotaxane.

■ ASSOCIATED CONTENT

Supporting Information

The Supporting Information is available free of charge at https://pubs.acs.org/doi/10.1021/acs.macromol.3c02606.

Figures S1−S8 (PDF)

■ AUTHOR INFORMATION

Corresponding Authors

Xiang-Meng Jia − *South China Advanced Institute for Soft Matter Science and Technology, School of Emergent Soft Matter, South China University of Technology, Guangzhou 510640, China; Guangdong Provincial Key Laboratory of Functional and Intelligent Hybrid Materials and Devices, South China University of Technology, Guangzhou 510640, China;* Present Address: Shandong Laboratory of Advanced Materials and Green Manufacturing at Yantai; orcid.org/0000-0002-4056-747X; Email: jiaxm@scut.edu.cn

Jiajia Zhou − *South China Advanced Institute for Soft Matter Science and Technology, School of Emergent Soft Matter, South China University of Technology, Guangzhou 510640, China; Guangdong Provincial Key Laboratory of Functional and Intelligent Hybrid Materials and Devices, South China University of Technology, Guangzhou 510640, China;* orcid.org/0000-0002-2258-6757; Email: zhouj2@scut.edu.cn

Authors

Jinyuan Mao − *South China Advanced Institute for Soft Matter Science and Technology, School of Emergent Soft Matter, South China University of Technology, Guangzhou 510640, China; Guangdong Provincial Key Laboratory of Functional and Intelligent Hybrid Materials and Devices, South China University of Technology, Guangzhou 510640, China;* orcid.org/0000-0003-2496-777X

Guojie Zhang − *Department of Chemical Engineering, School of Chemistry and Chemical Engineering, Guangzhou University, Guangzhou 510006, China*

Complete contact information is available at: https://pubs.acs.org/10.1021/acs.macromol.3c02606

Notes

The authors declare no competing financial interest.

■ ACKNOWLEDGMENTS

We acknowledge the support of the National Key R&D Program of China (2022YFE0103800) and the National Natural Science Foundation of China (21774004, 22373036). The computation was made possible by the facilities of Information and Network Engineering and Research Center of SCUT.

■ REFERENCES

(1) Hart, L. F.; Hertzog, J. E.; Rauscher, P. M.; Rawe, B. W.; Tranquilli, M. M.; Rowan, S. J. Material properties and applications of mechanically interlocked polymers. *Nat. Rev. Mater.* **2021**, *6*, 508−530.

(2) Chen, L.; Sheng, X.; Li, G.; Huang, F. Mechanically interlocked polymers based on rotaxanes. *Chem. Soc. Rev.* **2022**, *51*, 7046−7065.

(3) Sauvage, J.-P. From chemical topology to molecular machines (Nobel Lecture). *Angew. Chem., Int. Ed.* **2017**, *56*, 11080−11093.

(4) Feringa, B. L. The art of building small: From molecular switches to motors (Nobel Lecture). *Angew. Chem., Int. Ed.* **2017**, *56*, 11060−11078.

(5) Stoddart, J. F. Mechanically interlocked molecules (MIMs)—molecular shuttles, switches, and machines (Nobel Lecture). *Angew. Chem., Int. Ed.* **2017**, *56*, 11094−11125.

(6) Cotí, K. K.; Belowich, M. E.; Liong, M.; Ambrogio, M. W.; Lau, Y. A.; Khatib, H. A.; Zink, J. I.; Khashab, N. M.; Stoddart, J. F. Mechanised nanoparticles for drug delivery. *Nanoscale* **2009**, *1*, 16−39.

(7) Zhang, J.; Ma, P. X. Cyclodextrin-based supramolecular systems for drug delivery: recent progress and future perspective. *Adv. Drug Delivery Rev.* **2013**, *65*, 1215−1233.

(8) Kwamen, C.; Niemeyer, J. Functional rotaxanes in catalysis. *Chemistry−A European Journal* **2021**, *27*, 175−186.

(9) Evans, N. H.; Beer, P. D. Progress in the synthesis and exploitation of catenanes since the Millennium. *Chem. Soc. Rev.* **2014**, *43*, 4658−4683.

(10) Leigh, D. A.; Marcos, V.; Wilson, M. R. Rotaxane catalysts. *ACS Catal.* **2014**, *4*, 4490−4497.

(11) Harrison, I. T.; Harrison, S. Synthesis of a stable complex of a macrocycle and a threaded chain. *J. Am. Chem. Soc.* **1967**, *89*, 5723−5724.
(12) Harada, A.; Li, J.; Kamachi, M. The molecular necklace: a rotaxane containing many threaded α-cyclodextrins. *Nature* **1992**, *356*, 325−327.
(13) Harada, A.; Li, J.; Nakamitsu, T.; Kamachi, M. Preparation and characterization of polyrotaxanes containing many threaded. alpha.-cyclodextrins. *Journal of Organic Chemistry* **1993**, *58*, 7524−7528.
(14) Sawada, J.; Aoki, D.; Otsuka, H.; Takata, T. A guiding principle for strengthening crosslinked polymers: Synthesis and application of mobility-controlling rotaxane crosslinkers. *Angew. Chem., Int. Ed.* **2019**, *58*, 2765−2768.
(15) Okumura, Y.; Ito, K. The polyrotaxane gel: A topological gel by figure-of-eight cross-links. *Adv. Mater.* **2001**, *13*, 485−487.
(16) Kato, K.; Yasuda, T.; Ito, K. Peculiar elasticity and strain hardening attributable to counteracting entropy of chain and ring in slide-ring gels. *Polymer* **2014**, *55*, 2614−2619.
(17) Kato, K.; Yasuda, T.; Ito, K. Viscoelastic properties of slide-ring gels reflecting sliding dynamics of partial chains and entropy of ring components. *Macromolecules* **2013**, *46*, 310−316.
(18) Hatakeyama, K.; Ishikawa, Y.; Kirihara, K.; Ito, T.; Mayumi, K.; Ito, K.; Terashima, K.; Hakuta, Y.; Shimizu, Y. Slide-ring material/highly dispersed graphene oxide composite with mechanical strength and tunable electrical conduction as a stretchable-base substrate. *ACS Appl. Mater. Interfaces* **2020**, *12*, 47911−47920.
(19) Ito, K. Novel cross-linking concept of polymer network: synthesis, structure, and properties of slide-ring gels with freely movable junctions. *Polym. J.* **2007**, *39*, 489−499.
(20) Ito, K. Slide-ring materials using topological supramolecular architecture. *Curr. Opin. Solid State Mater. Sci.* **2010**, *14*, 28−34.
(21) Mayumi, K.; Tezuka, M.; Bando, A.; Ito, K. Mechanics of slide-ring gels: Novel entropic elasticity of a topological network formed by ring and string. *Soft Matter* **2012**, *8*, 8179−8183.
(22) Kondo, Y.; Urayama, K.; Kidowaki, M.; Mayumi, K.; Takigawa, T.; Ito, K. Applicability of a particularly simple model to nonlinear elasticity of slide-ring gels with movable cross-links as revealed by unequal biaxial deformation. *J. Chem. Phys.* **2014**, *141*, 134906.
(23) Kato, K.; Karube, K.; Nakamura, N.; Ito, K. The effect of ring size on the mechanical relaxation dynamics of polyrotaxane gels. *Polym. Chem.* **2015**, *6*, 2241−2248.
(24) Hashimoto, K.; Shiwaku, T.; Aoki, H.; Yokoyama, H.; Mayumi, K.; Ito, K. Strain-induced crystallization and phase separation used for fabricating a tough and stiff slide-ring solid polymer electrolyte. *Science Advances* **2023**, *9*, No. eadi8505.
(25) Yasuda, Y.; Masumoto, T.; Mayumi, K.; Toda, M.; Yokoyama, H.; Morita, H.; Ito, K. Molecular dynamics simulation and theoretical model of elasticity in slide-ring gels. *ACS Macro Lett.* **2020**, *9*, 1280−1285.
(26) Kato, K.; Ikeda, Y.; Ito, K. Direct determination of cross-link density and its correlation with the elastic modulus of a gel with slidable cross-links. *ACS Macro Lett.* **2019**, *8*, 700−704.
(27) de Gennes, P.-G. Sliding gels. *Physica A: Statistical Mechanics and its Applications* **1999**, *271*, 231−237.
(28) Urayama, K.; Kawamura, T.; Kohjiya, S. Structure−mechanical property correlations of model siloxane elastomers with controlled network topology. *Polymer* **2009**, *50*, 347−356.
(29) Baulin, V. A.; Johner, A.; Marques, C. M. Sliding grafted polymer layers. *Macromolecules* **2005**, *38*, 1434−1441.
(30) Pinson, M. B.; Sevick, E. M.; Williams, D. R. Mobile rings on a polyrotaxane lead to a yield force. *Macromolecules* **2013**, *46*, 4191−4197.
(31) Müller, T.; Sommer, J.-U.; Lang, M. Tendomers-force sensitive bis-rotaxanes with jump-like deformation behavior. *Soft Matter* **2019**, *15*, 3671−3679.
(32) Müller, T.; Sommer, J.-U.; Lang, M. Swelling of tendomer gels. *Macromolecules* **2021**, *54*, 4601−4614.
(33) Müller, T.; Sommer, J.-U.; Lang, M. Elasticity of tendomer gels. *Macromolecules* **2022**, *55*, 7540−7555.
(34) Kremer, K.; Grest, G. S. Dynamics of entangled linear polymer melts: A molecular-dynamics simulation. *J. Chem. Phys.* **1990**, *92*, 5057−5086.
(35) Zhu, Y.; Liu, H.; Li, Z.; Qian, H.; Milano, G.; Lu, Z. GALAMOST: GPU-accelerated large-scale molecular simulation toolkit. *J. Comput. Chem.* **2013**, *34*, 2197−2211.
(36) Weeks, J. D.; Chandler, D.; Andersen, H. C. Role of repulsive forces in determining the equilibrium structure of simple liquids. *J. Chem. Phys.* **1971**, *54*, 5237−5247.
(37) Yasuda, Y.; Toda, M.; Mayumi, K.; Yokoyama, H.; Morita, H.; Ito, K. Sliding dynamics of ring on polymer in rotaxane: A coarse-grained molecular dynamics simulation study. *Macromolecules* **2019**, *52*, 3787−3793.
(38) Uehara, S.; Wang, Y.; Ootani, Y.; Ozawa, N.; Kubo, M. Molecular-level elucidation of a fracture process in slide-ring gels via coarse-grained molecular dynamics simulations. *Macromolecules* **2022**, *55*, 1946−1956.
(39) Rubinstein, M.; Colby, R. H. *Polymer Physics*; Oxford University Press: New York, 2003.

https://doi.org/10.1021/acs.macromol.3c02606
Macromolecules 2024, 57, 3841−3849

Supporting Information: Excluded Volume of Slide Rings in Single-chain Polyrotaxane

Jinyuan Mao,[†,‡] Xiang-Meng Jia,[*,†,‡] Guojie Zhang,[¶] and Jiajia Zhou[*,†,‡]

†*South China Advanced Institute for Soft Matter Science and Technology, School of Emergent Soft Matter, South China University of Technology, Guangzhou 510640, China*

‡*Guangdong Provincial Key Laboratory of Functional and Intelligent Hybrid Materials and Devices, South China University of Technology, Guangzhou 510640, China*

¶*Department of Chemical Engineering, School of Chemistry and Chemical Engineering, Guangzhou University, Guangzhou 510006, China*

E-mail: jiaxm@scut.edu.cn; zhouj2@scut.edu.cn

This PDF file includes:

Figures S1-S8.

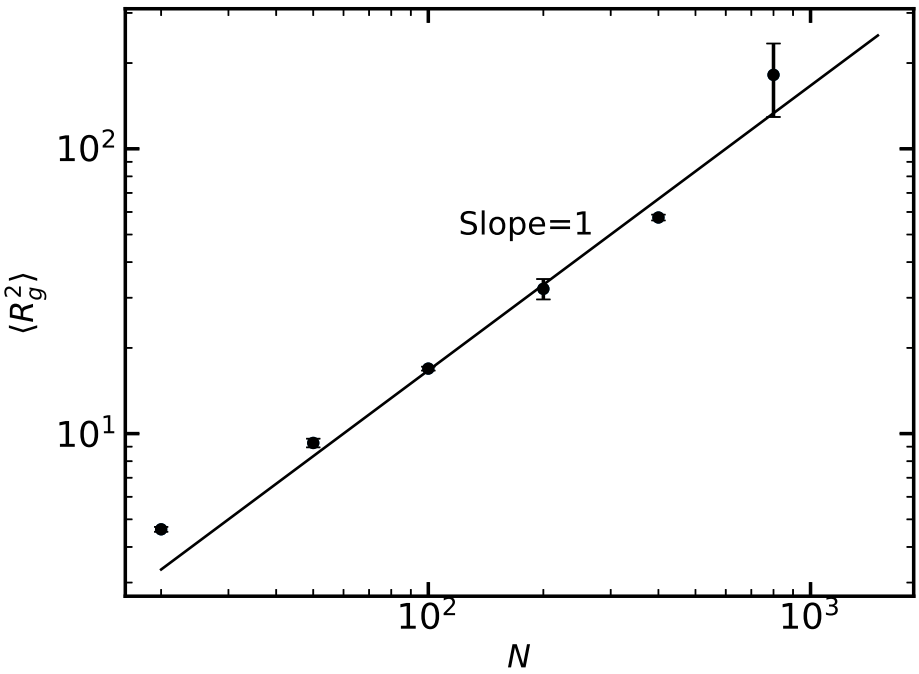

Figure S1: The relationship between $\langle R_g^2 \rangle$ and N of a single-chain polyrotaxane without slide rings.

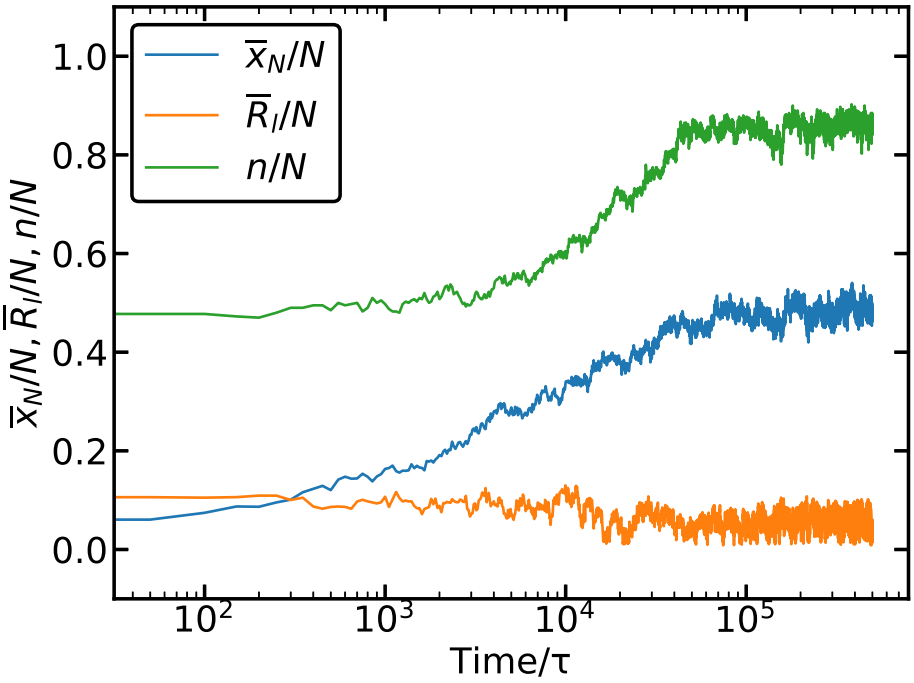

Figure S2: Time series of $\bar{x}_N$, $\bar{R}_l$ and n for $p20b20$ under the applied force of $\bar{f} = 2.0$.

According to Figure **S3**, the radius of rings (R) was calculated using the average bond length (r). Therefore, the excluded volume $\bar{\text{v}}$ can be calculated as $\bar{\text{v}}a^3 = 4\pi R^3/3$. In our simulation, the average bond length is $r = 0.97\,\sigma$, which yields $R \approx 1.62\,\sigma$. Therefore, the excluded volume $\bar{\text{v}}$ could be estimated as $\bar{\text{v}} \approx 17.7$.

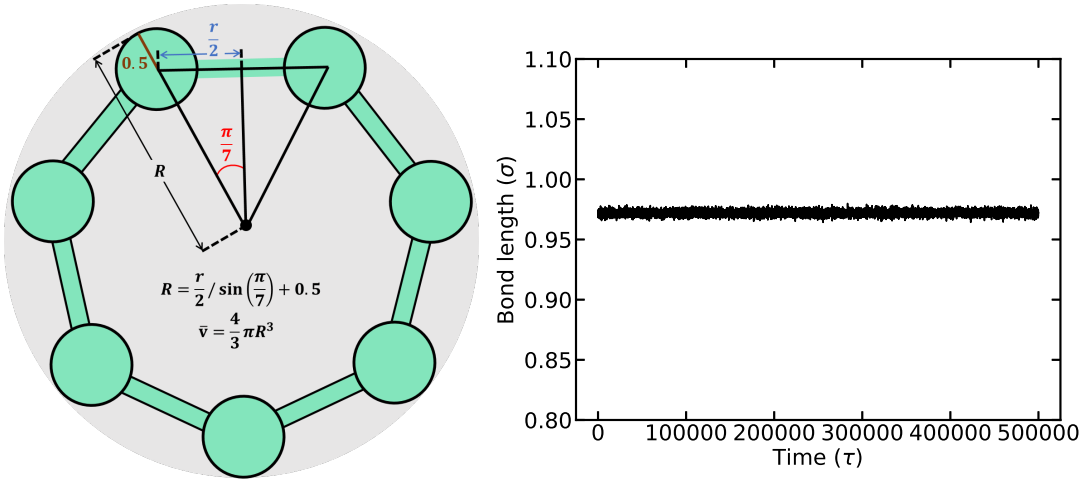

Figure S3: Left: The derivation of the approximate radius of rings. Right: The average bond length of "p20b20" scenario under the applied force of $\bar{f} = 2.0$.

Figures **S4** and **S5** show the simulation results for asymmetric distributions, and the comparison with the theory in section "$p \neq 0$, $b \neq 0$ without excluded volume of slide rings".

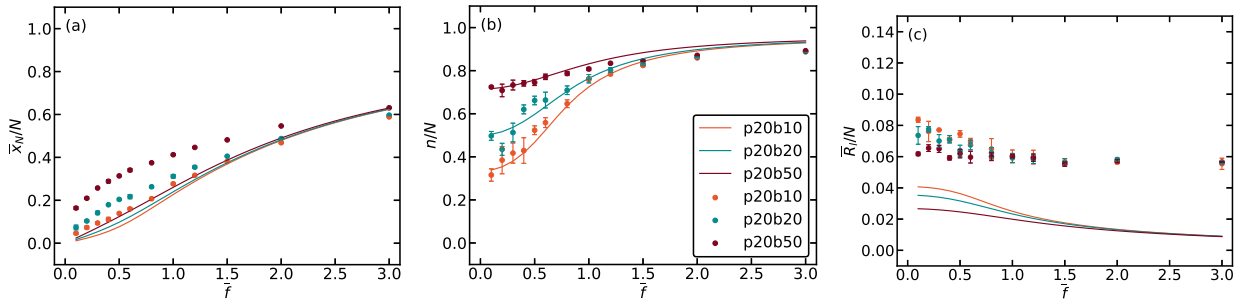

Figure S4: Theoretical predictions (solid line) without the excluded volume effects of both p and b rings, and simulation results (dots) are presented for a single-chain polyrotaxane model in a Θ solvent when $p = 20$ and $b = 10, 20, 50$. (a) Dimensionless projection of the end-to-end distance in the direction of the applied force ($\bar{x}_N$) as a function of the dimensionless applied force ($\bar{f}$). (b) Number of monomers (n) on the force side as a function of $\bar{f}$. (c) Dimensionless end-to-end distance ($\bar{R}_l$) on the free side as a function of $\bar{f}$. The solid line in (c) represents the expected behavior of the Gaussian chain, specifically $\langle \bar{R}_l^2 \rangle^{1/2} \sim (N-n)^{1/2} a$.

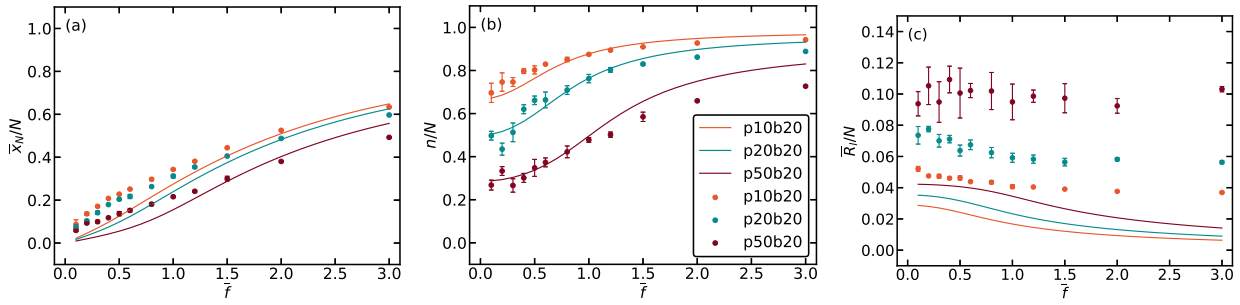

Figure S5: Theoretical predictions (solid line) without the excluded volume effects of both p and b rings, and simulation results (dots) are presented for a single-chain polyrotaxane model in a Θ solvent when $b = 20$ and $p = 10, 20, 50$. (a) Dimensionless projection of the end-to-end distance in the direction of the applied force ($\bar{x}_N$) as a function of the dimensionless applied force ($\bar{f}$). (b) Number of monomers (n) on the force side as a function of $\bar{f}$. (c) Dimensionless end-to-end distance ($\bar{R}_l$) on the free side as a function of $\bar{f}$. The solid line in (c) represents the expected behavior of the Gaussian chain, specifically $\langle \bar{R}_l^2 \rangle^{1/2} \sim (N-n)^{1/2} a$.

Figures **S6** and **S7** show the simulation results for asymmetric distributions, and the comparison with the theory in section "$p \neq 0$, $b \neq 0$ with excluded volume of slide rings".

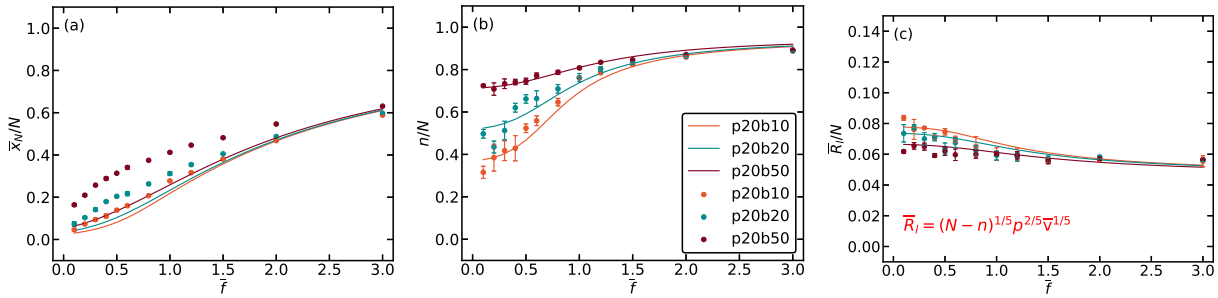

Figure S6: Theoretical predictions (solid line) with the excluded volume effects of both p and b rings, and simulation results (dots) are presented for a single-chain polyrotaxane model in a Θ solvent when $p = 20$ and $b = 10$, 20, 50. (a) Dimensionless projection of the end-to-end distance in the direction of the applied force ($\bar{x}_N$) as a function of the dimensionless applied force ($\bar{f}$). (b) Number of monomers (n) on the force side as a function of $\bar{f}$. (c) Dimensionless end-to-end distance ($\bar{R}_l$) on the free side as a function of $\bar{f}$. The solid line in (c) represents values derived from the equation $\bar{R}_l = (N-n)^{1/5} p^{2/5} \bar{\nu}^{1/5}$ as given in Eq. (31), with $\bar{\nu} \approx 17.7$.

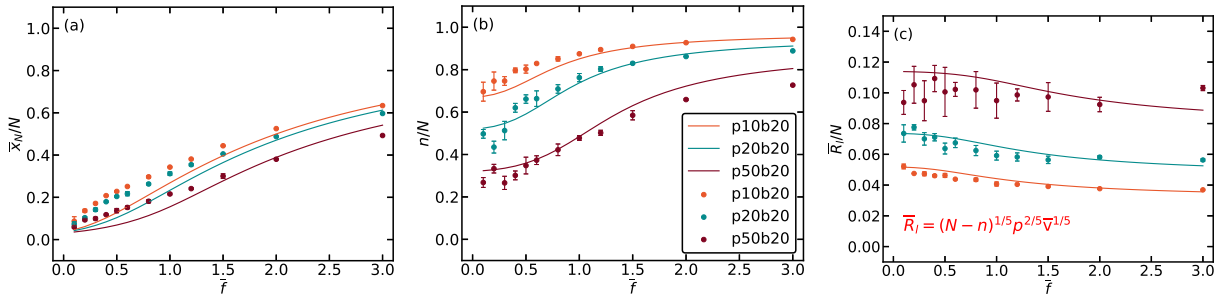

Figure S7: Theoretical predictions (solid line) with the excluded volume effects of both p and b rings, and simulation results (dots) are presented for a single-chain polyrotaxane model in a Θ solvent when $b = 20$ and $p = 10$, 20, 50. (a) Dimensionless projection of the end-to-end distance in the direction of the applied force ($\bar{x}_N$) as a function of the dimensionless applied force ($\bar{f}$). (b) Number of monomers (n) on the force side as a function of $\bar{f}$. (c) Dimensionless end-to-end distance ($\bar{R}_l$) on the free side as a function of $\bar{f}$. The solid line in (c) represents values derived from the equation $\bar{R}_l = (N-n)^{1/5} p^{2/5} \bar{\nu}^{1/5}$ as given in Eq. (31), with $\bar{\nu} \approx 17.7$.

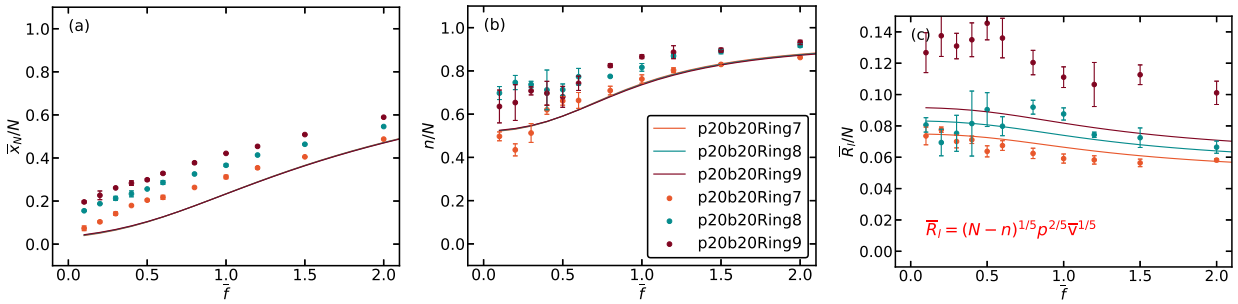

Figure S8: Theoretical predictions for different ring radius (solid line), and simulation results (dots) for a single-chain polyrotaxane model in a Θ-solvent for $p20b20$. (a) Dimensionless projection of the end-to-end distance in the direction of the applied force ($\bar{x}_N$) as a function of the dimensionless applied force ($\bar{f}$). (b) Number of monomers (n) on the force side as a function of $\bar{f}$. (c) Dimensionless end-to-end distance ($\bar{R}_l$) on the free side as a function of $\bar{f}$.